JYX
JYVÄSKYLÄN YLIOPISTO
UNIVERSITY OF JYVÄSKYLÄ

This is a self-archived version of an original article. This version may differ from the original in pagination and typographic details.

Author(s): Christophliemk, M. P.; Heponiemi, A.; Kangas, T.; Hu, T.; Prokkola, H.; Lassi, U.

Title: The catalytic wet air oxidation of pharmaceutical wastewater with alkali-activated Mn and Cu composites : preparation of precursors by calcination of kaolin with Mn and Cu

Year: 2024

Version: Published version

Copyright: © The Author(s) 2024

Rights: CC BY 4.0

Rights url: https://creativecommons.org/licenses/by/4.0/

Please cite the original version:

Christophliemk, M. P., Heponiemi, A., Kangas, T., Hu, T., Prokkola, H., & Lassi, U. (2024). The catalytic wet air oxidation of pharmaceutical wastewater with alkali-activated Mn and Cu composites : preparation of precursors by calcination of kaolin with Mn and Cu. Advanced Composites and Hybrid Materials, 7, Article 158. https://doi.org/10.1007/s42114-024-00982-8

Advanced Composites and Hybrid Materials (2024) 7:158
https://doi.org/10.1007/s42114-024-00982-8

RESEARCH

The catalytic wet air oxidation of pharmaceutical wastewater with alkali-activated Mn and Cu composites: preparation of precursors by calcination of kaolin with Mn and Cu

M. P. Christophliemk[1] · A. Heponiemi[1] · T. Kangas[1] · T. Hu[1] · H. Prokkola[1] · U. Lassi[1,2]

Received: 28 October 2023 / Revised: 28 June 2024 / Accepted: 21 September 2024
© The Author(s) 2024

Abstract

In recent decades, the concentration of pharmaceutical residues and narcotics has increased in municipal wastewater. Decomposing these toxic organic chemicals is challenging and requires new techniques and advanced catalytic materials. Precursors of metal composites were prepared by calcining an aqueous suspension of natural clay–based kaolin with Mn and Cu, binding chemically the active metals to the aluminosilicate frame structure of the precursor. The specific surface area of Mn and Cu composite was 67 m^2/g and 81 m^2/g, respectively. The mechanical durability was determined in terms of compressive strength, and 3.3 MPa and 3.6 MPa were obtained, respectively. In the CWAO of pharmaceutical wastewater, Mn composite gave the highest conversions of 54% and 46% of the chemical oxygen demand (COD) and total organic carbon (TOC), respectively. Metal composites were mechanically and chemically highly durable, inducing only 1.2 wt.% and 1.4 wt.% mass loss. In CWAO, Mn and Cu composite increased the biodegradation of organic species in the wastewater by 65% and 75%, respectively.

Keywords Metakaolin · Alkali-activated material · Transition metal · Catalytic wet air oxidation · Pharmaceutical wastewater

1 Introduction

Globally, the research and production of diverse medicinal products have been growing for some time. Also, in wastewater, the concentration of dissolved pharmaceutical and narcotic residues has grown in recent decades, which is a clear health threat to humans and the entire environment. Discharges of drug residues from several diverse sources (the pharmaceutical industry, hospitals, households, and research activities) occur much faster than their repair or automatic decomposition [1]. Because wastewater treatment plants are designed to process easily and moderately degradable organic compounds, they are unable to fully decompose pharmaceuticals. High stability, low biodegradability, and high lipophilicity are generally typical of pharmaceutical compounds [2]. Various methods and technical solutions are constantly being researched to remove residues from water, focusing on water treatment efficiency, current emission standards, and environmental limitations [3]. These residues are excreted directly from users and have already been detected in drinking water and in the human bloodstream. For example, bisphenol A

Highlights
- Ecological and low-cost porous metakaolin-based alkali-activated composites with nonnoble active metals (Mn composite and Cu composite) were produced for the wet air oxidation (CWAO) of pharmaceutical wastewater.
- In CWAO, Mn composite gave the highest conversions of 54% and 46% of the chemical oxygen demand (COD) and total organic carbon (TOC), respectively.
- Both Mn composite and Cu composite significantly increased the biodegradation of organic species in the wastewater by 65% and 75%, respectively.
- Metal composites were mechanically and chemically highly durable, inducing only 1.2 wt.% and 1.4 wt.% mass loss.

✉ M. P. Christophliemk
mika.christophliemk@oulu.fi

[1] Research Unit of Sustainable Chemistry, University of Oulu, P.O. Box 4300, 90014 Oulu, Finland

[2] Kokkola University Consortium Chydenius, University of Jyväskylä, P.O. Box 567, 67701 Kokkola, Finland

Published online: 30 September 2024

(BPA, 4,4′-(propane-2,2-diyl)diphenol)) is typically used in the production of plastic materials. It is soluble to some extent in water, from which it can be transferred to food and wastewater [4].

The use of water as a medium in various industrial processes has increased the need to reduce or remove toxic organic compounds from process and wastewater streams [5]. Catalytic wet air oxidation (CWAO) is an economical, environmentally friendly, and advanced oxidation process for toxic, hazardous, and nonbiodegradable pollutants under mild conditions. For organic compounds, free radical (homolytic) and ionic (heterolytic) oxidation reaction mechanisms have been proposed in CWAO [6]. The homogeneous CWAO process effectively treats even high concentrations of organic wastewater, but since a catalyst cannot be recovered, secondary pollution occurs [7]. The heterogeneous CWAO process is effective even at low reaction temperatures and pressures, such as 100–160 °C and 1.5–5.6 MPa [8, 9].

Inexpensive and active catalysts with longer lifetimes and high mechanical and chemical stability are a significant factor in the development of new water treatment technologies compared to expensive precious metals such as gold, platinum, ruthenium, and silver, which are still commonly used as catalysts [10–12]. It should also be noted that even when inexpensive transition metals are used, they are often supported by another metal or metal oxide. As mentioned, a natural material is used in this research as a support, which is available everywhere where clay can be found.

A properly functioning and stable heterogeneous catalyst (composite) used in a water treatment process should not leak or increase the waste load. For decades, alkali-activated materials (AAMs) have been used in the construction industry either as an additive or as a replacement ingredient in concrete; therefore, the properties required of a material are completely different from wastewater treatment [13, 14]. As an alternative to expensive noble catalyst materials, such as Pt, Au, and Ru, this study prepared ecological porous metakaolin-based alkali-activated composites with active inexpensive transition metals (i.e., Mn and Cu composites) for the catalytic wet air oxidation (CWAO) of pharmaceutical wastewater. When cost-effective, environmentally friendly production processes are desired, catalyst carriers, such as composites, should be produced using inexpensive ecological precursors. Also, transition metals, such as Mn, Fe, Co, Ni, and Cu, should be preferred as active metals in composites. Metal oxides, such as CuO [15] and MnO_2 [16], are commonly used catalysts when organic compounds in wastewater are oxidized. One of the cheapest metal oxides is MnO_x, which is considered one of the most effective metal oxides with high activity in the gas phase [17], whereas the hydroxide form of Cu is an active and efficient catalyst for the decomposition of organic pollutants in the liquid phase [18] due to the catalytically active site of copper hydroxides [19, 20]. Also, a hybrid catalyst, such as Cu-Fe-kaolin, has been investigated by Adegbesan et al. [21].

Table 1 Analyses of the initial pharmaceutical wastewater: pH, EC, COD, TOC, and BOD

pH	EC (S/m)	COD (mg/L)	TOC (mg/L)	BOD (mg/L)
12–13	11–12	4100	1100	23

Properties such as compressive strength, specific surface area (SSA), pore volume (PV), and pore size distribution are essential when mechanically and chemically durable porous metal composites are designed and produced. In an extensive literature review, several studies have been found in which both noble and transition metal catalysts have been used in wastewater treatment. However, detailed studies on the use of ecological and inexpensive metakaolin-based metal composites in CWAO for wastewater treatment have not been found, which gives the research conducted in this current article a high novelty value. This paper details the preparation process of novel porous metal composites and their experimental tests on real pharmaceutical wastewater in CWAO. The composites consisted of heterogeneous transition metals, Mn and Cu, and an ecological metakaolin-based alkali-activated material as catalyst support (or carrier). As a result of the experimental tests conducted in CWAO, the performance of Mn and Cu composite on pharmaceutical wastewater was excellent, significantly increasing the biodegradation of organic species. The cost-effective CWAO process and the ecological metal composites with inexpensive active metals could significantly reduce the overall cost of water treatment processes, enabling this type of process even in countries where expensive processes and chemicals are not economically feasible. To our knowledge, this is the first time that alkali-activated materials are used as support materials for Cu and Mn catalysts in catalytic wet oxidation.

2 The experiment

2.1 Materials

Mn- and Cu-based precursors (Mn-MK and Cu-MK) were prepared by calcining a suspension of laboratory-grade washed white kaolin (VWR Chemicals, Belgium) and $MnSO_4{\cdot}H_2O$ and $CuSO_4{\cdot}5H_2O$ (pro-analysis, Merck, Darmstadt, Germany) at 750 °C. KOH pellets (Emsure®, Merck KGaA, Germany) and a 35 wt.% K_2SiO_3 solution (Sateenkaari Perinnetalo, Finland) were used to prepare an alkaline activating solution. A solution of 30 wt.% H_2O_2 (AnalR NORMAPUR, VWR Chemicals, France) was used as a foaming agent to generate porosity in Mn and Cu composites. The wastewater was supplied by a

local pharmaceutical company in Finland. Table 1 presents the analysis of the initial pharmaceutical wastewater, such as pH, electrical conductivity (EC), chemical oxygen demand (COD), total organic carbon (TOC), and biological oxygen demand (BOD).

2.2 Preparation of precursors and metal composites

The precursors were produced by suspending 150 mL of aqueous solution of 0.5M $MnSO_4 \cdot H_2O$ and 0.5M $CuSO_4 \cdot 5H_2O$ with 200 g of powdered laboratory-grade kaolin. The suspensions were calcinated at 750 °C for 2 h to produce solid precursors (Mn-MK and Cu-MK) [22] and ground into a fine powder with a disk sieve. The powder was mixed by hand until it was as homogeneous as possible.

The porous metal composites were prepared in a reaction vessel of 300 mL by gradually adding powdered precursor within the alkaline activation solution of K_2SiO_3 and KOH under an effective mixing at 800 rpm for 10 min. The reaction vessel was connected to an IKA RW 20 digital overhead stirrer (IKA®-Werke GmbH & Co. KG, Germany) with an R 1382 three-bladed propeller stirrer (IKA®-Werke GmbH & Co. KG, Germany). The composition of the paste consisted of the following molar ratios of active substances: $SiO_2:K_2O = 8.8$, $SiO_2:Al_2O_3 = 4.2$, $Al_2O_3:K_2O = 2.1$, and $H_2O:K_2O = 16$. To achieve the desired porosity of the metal composites, a 2.5 wt.% foaming agent (30 wt.% H_2O_2) was added to the paste. Until all the ingredients were added, the paste was allowed to homogenize during mixing for another 10 min at 800 rpm. The ready-made paste was poured into a sealed Teflon cylinder and placed in a microwave oven for curing at 180 W for 10 min. The Teflon cylinder was sealed tightly so that the internal pressure formed by the hot water vapor would cause the gas bubbles to be evenly distributed around the cured metal composites. Finally, the porous durable metal composites were washed with distilled water for 5 min and dried overnight in an oven at 50 °C.

The reference materials, blank metakaolin (B-MK) and blank metakaolin–based alkali-activated material (B-MK-AAM), were prepared as described in the previous paragraph with the same molar ratios of active substances, but without active metal. Laboratory-grade kaolin was calcined at 750 °C for 2 h to produce B-MK. A blank metakaolin-based alkali-activated material (B-MK-AAM) was prepared by gradually adding ground B-MK to the alkaline activation solution of K_2SiO_3 and KOH with efficient mixing. During mixing, a blowing agent (30 wt% H_2O_2) (2.5 wt%) was added to the paste to provide porosity for B-MK-AAM [23–25].

2.3 Characterization methods of metal composites

The porosity of the metal composites was determined by nitrogen physisorption measurements using a Micromeritics ASAP 2020 instrument (Micromeritics Instruments; Norcross, GA, USA). The SSA was determined based on the nitrogen physisorption isotherms measured at −196 °C. The adsorption isotherms were obtained by immersing the sample tubes in liquid nitrogen (−196 °C) to achieve constant temperature conditions and by adding a small dose of gaseous nitrogen to the samples. The SSA, mean pore diameter (MPD), PV, and pore size distribution were determined using BET (RSD ± 5%) and nonlocal density functional theory (NLDFT) models [26], which are based on the model of independent slit-shaped pores specifically tailored to structured materials [27].

The mechanical durability or compressive strength of the metal composites was measured by a Zwick/Roell TestControl-II v7.62 type BW91272 unit (Zwick/Roell, Germany) equipped with a Tesproma compression unit (Tesproma, Finland). The measured data was collected using the testXpert II-V3.6 software. In all measurements, the compressive force was 9 kN, and the driving speed was 0.1 mm/s. The measurement stopped automatically when 25% of the sample was deformed. For both composites, the compressive strength was remeasured three times, and the average compressive strength was determined.

X-ray fluorescence spectrometer (XRF) was performed to detect the active metal content (wt.%) of the precursors (Mn-MK and Cu-MKs) and the metal composites by a high-power wavelength dispersive X-ray fluorescence spectrometer (XRF) (PANalytical Axios mAX 4 kW WDXRF, Almelo, The Netherlands). The measurements were performed using loose powders placed in a transparent Mylar film in a He atmosphere.

Inductively coupled plasma optical emission spectroscopy (ICP-OES) was conducted to analyze the metal content in the metal components by (ICP-OES; Agilent 5110 SVDV; Agilent Technologies Inc., Santa Clara, CA, USA).

X-ray diffractometer (XRD) was performed to investigate the crystal phases of the metal composites by X-ray diffractometer (XRD) (PANalytical X'Pert Pro XRD, Almelo, The Netherlands) using monochromatic Cu Kα1 ($\lambda = 1.5406$ Å) at 45 kV and 40 mA at a scan speed of 0.017°/s and 2θ ranging from 8–85°. The diffractograms were analyzed using HighScore Plus software (version 4.0, PANalytical B. V., Almelo, The Netherlands) using the Powder Diffraction File standards obtained from the International Centre for Diffraction Data (ICDD).

X-ray photoelectron spectroscopy (XPS) was performed to analyze the elemental composition and binding states of the active metals of Mn and Cu composite by Thermo Fisher Scientific ESCALAB 250Xi XPS System (Thermo Fisher

Scientific, 168 Third Avenue, Waltham, MA, 02451, USA) at the University of Oulu's (Finland) Center for Material Analysis. The sample powders were placed in a gold sample holder. With pass energy of 20 eV and a spot size of 900 µm, Cu, Mn, and C were measured for the composites. The measurement data were analyzed using Avantage V5 software. The monochromatic AlKα radiation (1486.7 eV) was operated at 20 mA and 15 kV. Charge compensation was used to determine the presented spectra, and the binding energies were calibrated by applying the C1s line at 284.8 eV as a reference. Gaussian multipeak fitting was used to determine the cumulative curves.

Raman spectroscopy was conducted to investigate detailed information about the chemical structures and molecular interactions of metal composites by a time-gated PicoRaman spectrometer from Timegate Instruments Ltd. (Oulu, Finland). The measurements were done between a wave number range of 100–2100 cm^{-1} with ~ 5 cm^{-1} spectral resolution, and the samples were rotated during the measurements. PicoRaman uses a 532-nm pulsed laser with a shot length of 150 ps and a frequency of 40–100 kHz. Gaussian multipeak fitting was used to determine the cumulative curves.

Elemental mapping and composition analysis were performed via field emission scanning electron microscope-energy-dispersive X-ray spectroscopy (FESEM-EDS) analysis using a Zeiss Ultra Plus (Carl Zeiss Microscopy GmbH, Jena, Germany) with Aztec software of Oxford Instruments at the Centre for Material Analysis at the University of Oulu. The EDS analysis was operated at 15 kV, and the working distance was 8.5 mm.

2.4 Catalytic wet air oxidation

The catalytic wet air oxidation (CWAO) experiments were performed using a 300-mL high-pressure Hastelloy C22 stainless steel reactor (Parr, Moline, IL, USA) and loaded with 160 mL of pharmaceutical wastewater (pH 12–13) while mixing at 500 rpm. The selected parameters were reactor temperature (185 °C), air pressure (6.0 MPa), and catalyst load (4.0 g/L). The metal composites were weighed and placed in a static catalyst basket (Parr) in the reactor. To begin, the reactor was purged with pressurized nitrogen gas while heating to the desired reaction temperature (185 °C). When the set reaction temperature was achieved, the nitrogen gas flow was stopped, and technical air was introduced into the pressured reactor. Intermediate samples (11 pcs.) were collected as a function of oxidation time (minutes 20, 40, 50, 60, 90, 120, 150, 180, 200, 240, and 300), and variations in pH were monitored.

The CWAO was conducted in two ways: (a) to ensure reproducibility, the experiments were repeated three times with the initial process wastewater and metal composites, and (b) to investigate the reusability and activity of the metal composites, the oxidation was conducted four times and always with fresh initial wastewater, but the same Mn and Cu composites. As a reference, oxidation was conducted as a gas-liquid system without an added metal composite (WAO). After CWAO, metal composites were washed with distilled water and dried overnight in an oven at 60 °C for further analysis. During the experiments, the COD, TOC, and BOD of the initial and processed process wastewater samples were monitored. The chemical stability of the metal composites was investigated by monitoring the leaching of any active metals into the pharmaceutical wastewater samples using inductively coupled plasma optical emission spectroscopy ICP-OES (Agilent 5110 SVDV; Agilent Technologies Inc., Santa Clara, CA, USA). The pseudo-first order rate law was fitted to the experimental COD conversion (%) results of process wastewater for the metal composites by using a standard nonlinear least squares algorithm. The pseudo-first-order rate law is shown in Eq. 1 [28]:

$$R(t) = R_{\text{tot}}(1 - e^{-kt}) \tag{1}$$

where t refers to the time of oxidation and total conversion (R_{tot}) and rate constant (k) were used as fitting parameters.

2.5 Characterization methods of pharmaceutical wastewater

COD measurements were used to monitor the decomposition of organic species in pharmaceutical wastewater with Standard Method 5220D: closed reflux, colorimetric method using Hach Lange cuvette tests (APHA 2012). Dichromate ion ($Cr_2O_7^{2-}$) is defined as an oxidizer in Method 5220D, which is reduced to chromium ion (Cr^{3+}). The organic and inorganic species of the solution are susceptible to oxidation. The green coloration of the Cr^{3+} was measured by a Hach Lange DR 2800 spectrometer at a wavelength of 605 nm (APHA 2012). TOC was used to determine the content of organic carbon in the treated wastewater samples with a Shimadzu TOC-LCSH (Shimadzu Corporation, Kyoto, Japan) TOC Analyzer fitted with magnetic stirring capability. TOC was also needed with BOD to determine the degree of biodegradation of the wastewater. The TOC content was calculated as the mean of three replicate measurements via the TC-IC method, and the calibration of the instrument was verified using niacin solutions with carbon contents of 80% and 20%, respectively, of the highest calibration standard. Before analysis, the particle size of the solids was reduced to aid with sample homogeneity using an ultrasound homogenizer Bandelin SONOPULS HD 4200 (Bandelin Electronic GmbH Co., KG, Berlin, Germany) fitted with a SONOPULS TS 103 sonotrode for 1 min at 20% power.

BOD was determined before and after CWAO (initial and terminal samples) using the manometric respirometric BOD OxiTop® technique, which is based on an automated pressure measurement in a closed system and constant temperature (20 ± 0.2 °C). Biodegradability was determined using BOD OxiTop equipment (BOD OxiTop C110 (WTW, Xylem Analytics UK Ltd., 2006, England). During biodegradation, a sample consumes O_2 (g), producing water and CO_2, which is absorbed into NaOH granules. The BOD was measured automatically based on the ideal gas law modified for conditions in a closed environment.

In this current study, for both composites, BOD was measured for 28 days; for Cu composite, the measurement continued for another 14 days to achieve a stable response for BOD.

Theoretical oxygen demand (ThOD) was calculated based on the BOD and TOC results (Eq. 2) [29]:

$$\mathrm{ThOD} = c(\mathrm{C})\frac{M(\mathrm{O_2})}{M(\mathrm{C})} \tag{2}$$

where c(C) is the TOC of the process wastewater (g/L), $M(O_2)$ is the molecular weight of oxygen (32 g/mol), and M(C) is the molecular weight of carbon (12 g/mol). The degree of biodegradation is given as the ratio of BOD to ThOD (Eq. 3) [29]:

$$\text{Degree of biodegradation (\%)} = \frac{\mathrm{BOD}}{\mathrm{ThOD}} \times 100\% \tag{3}$$

3 Results and discussion

3.1 Porosity and mechanical strength

The porosity of metal composites plays a significant role as a support (or carrier) for active metals. When the porosity is homogenously distributed, even more active metals can be bound into the structure of the metal composites, which increases catalytic activity. Also, the average compressive strength (ACS) of metal composites was determined with a compressive force of 9 kN and a driving speed of 0.1 mm/s, respectively. B-MK-AAM without added active metal was used as a reference. All the materials' porosity and durability data are presented in Table 2.

As Nyborg and Cao studied the surface properties of pure copper powder [30], this current study also determined the SSA of active metal powders, obtaining 20 m^2/g for Mn and 151 m^2/g for Cu. It is being proposed that these partial SSAs of active metals could increase the total SSA of the metal composites. The N_2 adsorption-desorption isotherms of the initial Mn and Cu composite were determined by introducing type IV isotherms with distinguishing hysteresis loops corresponding to mesoporous materials (see 1. Supplementary Material: Isotherm of Initial Mn and Cu composite). This can also be observed in Table 2, where the mesopores (2.2 – 50 nm) have the highest pore size distribution.

The metal composites were prepared by curing the paste in a microwave oven at 190 W for 10 min to increase the mechanical durability of metal composites. Microwave radiation (i.e., electromagnetic radiation) has been reported to increase mechanical durability by affecting the crystal structure of a material [31, 32]. Electromagnetic radiation enables even faster heating due to interactions between polar molecules and a microwave's electric fields [33]. Based on a study by Chindaprasirt et al., in the initial phase of radiation, a microwave promotes the dissolution of Si and Al species, enhancing the formation of a gel that breaks the hydrogen bonds of water molecules. Gel formation on the MK particles might cause greater densification of the matrix [34]. Also, active metals could increase the mechanical durability of metal composites when they are bound to the Si and Al frameworks of metal composites. As a result, the compressive strength of metal composites was appropriate for the reaction conditions of CWAO at 6.0 MPa with 500 rpm mixing.

3.2 X-ray fluorescence

X-ray fluorescence (XRF) was used to monitor possible variations in the metal content of Mn- and Cu-MK and metal composites. It is essential that the content (wt.%) of Si, Al, K, Mn, and Cu remains within the limits so that the structure of the composites is mechanically and chemically stable.

Table 2 Porosity and compressive strength of blank B-MK-AAM and Mn and Cu composite

Material	SSA (m^2/g)	MPD (nm)	PV (cm^3/g)	Micropores (< 2.2 nm)	Mesopores (2.2 – 50 nm)	Macropores (> 50 nm)	ACS (MPa)
				Pore size distribution (%)			
B-MK-AAM	42	5.2	0.1	10	77	13	2.8
Mn composite	67	8.8	0.2	4.5	92	3.5	3.3
Cu composite	81	10	0.2	6.0	76	18	3.6

SSA specific surface area, *MPD* mean pore diameter, *PV* total pore volume, *ACS* average compressive strength

The metal content (wt.%) of B-MK (reference), B-MK-AAM (reference), Mn- and Cu-MK, and metal composites was determined. The analyzed metals are reported as elements in Table 3. The active metal content (wt.%) of Mn- and Cu-MK and metal composites predictably increased compared to the references. When compared to B-MK and Mn- and Cu-MK, the content of K (wt.%) was increased in B-MK-AAM and metal composites due to the addition of K_2SiO_3 and KOH during the preparation of the alkali-activated paste.

3.3 X-ray photoelectron spectroscopy

The purpose of the XPS analysis was to determine the oxidation state of active metals in metal composites. The XPS survey scan analysis was carried out in the binding energy range of 0–1347 eV (see 2. Supplementary Material: XPS Survey Scan of Mn and Cu composite). Figure 1 shows the (a) Mn composite Mn2p spectra and (b) Cu composite Cu2p spectra [35–37]. The energy levels of Mn2p, Mn3s, and Mn3p were obtained in the energy locations, as reported [36, 38]. As can be seen, the spin-energy difference of 12 eV (a) and 20 eV (b) agrees with the reported data for $Mn2p_{3/2}$, $Mn2p_{1/2}$ of MnO_2 [39], $Cu(OH)_2$, and Cu_2O [35, 40, 41]. Based on the XPS analysis, the presence of Mn_3O_4, $Cu(OH)_2$, Cu_2O, and metallic Cu(0) in metal composites was confirmed [35].

Figure 2 presents the Mn3s peaks of the Mn_3O_4 (Mn composite) [36] and the possible oxide compositions of $2MnO \cdot MnO_2$ [12, 26], which is proposed to interact with the silica groups of Mn composite [42]. Also, the formation of Mn_3O_4 during the calcination of kaolin and $MnSO_4 \cdot H_2O$ (aq) is detailed later in this paper.

Table 3 XRF analysis of the metal content (wt.%) in B-MK (reference), B-MK-AAM (reference), Mn- and Cu-MK (precursor), Mn composite, and Cu composite

Materials	Al wt.%	Si	K	Cu	Mn
B-MK	21	31	1.5	< 1.0	< 1.0
B-MK-AAM	12	19	4.3	< 1.0	< 1.0
Mn-MK	20	30	1.4	< 1.0	8.2
Cu-MK	19	29	1.5	9.8	< 1.0
Mn composite	13	20	4.0	< 1.0	8.1
Cu composite	13	20	5.0	9.6	< 1.0

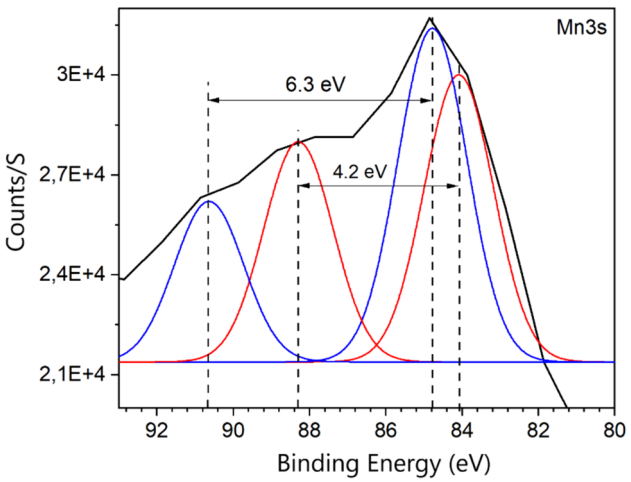

Fig. 2 Fitted XPS spectra of Mn_3O_4 (Mn composite), Mn3s regions fitted for Mn^{2+} and Mn^{4+}

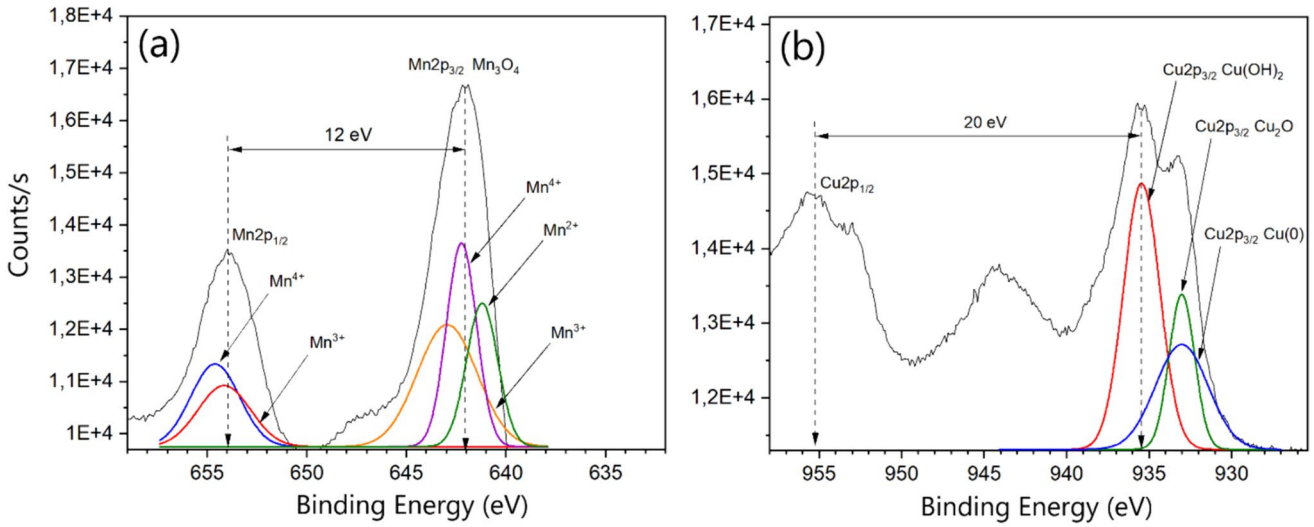

Fig. 1 **a** Mn2p spectra of Mn_3O_4 and **b** Cu2p spectra of $Cu(OH)_2$, Cu_2O, metallic Cu(0) (Mn and Cu composite)

3.4 Raman spectroscopy

The bands of Si/SiO_2 (in spectra marked as black) and Al_2O_3 (in spectra marked as blue) in both Mn and Cu composite are presented in Fig. 3a, b. Detailed spread Raman shifts of (a) Mn composite and (b) Cu composite (Mn–O–Si and Cu–O–Si) are presented in Fig. 4a, b, with the cumulative curve of Gaussian multipeak fitting. Raman spectroscopy bands of Si/SiO_2 and Al_2O_3 species in metal composites are presented in Table 4.

Detailed structures of Mn–Si–O and Cu–Si–O between 100 and 700 cm^{-1} were studied by performing Gaussian multipeak fitting. Mn composite (Fig. 4a) showed three overlapped bands (610, 648, and 685 cm^{-1}), which were proposed as a Mn_5Si_3 phase [47]. Also, a set of three bands at 267* (shoulder), 293, and 320 cm^{-1} were proposed to Mn–Si, where the band 367 cm^{-1} was covered by broad overlapped signals [48]. The strong peak at 440 cm^{-1} was proposed to originate from the bending modes of Si-O-Al and Si-O-Si, respectively [49]. Cu composite (Fig. 4b) has a single band at 139 cm^{-1}, which was introduced to Cu_2O. CuO should be seen at 284 and 628 cm^{-1}, which slightly differs from the reported data (296, 630 cm^{-1}) [50]. Also, the mixed phase of CuO/Cu_2O was reported to be located at 628–630 cm^{-1}. The band at 628 cm^{-1} (reported value 630 cm^{-1}) [50] was introduced

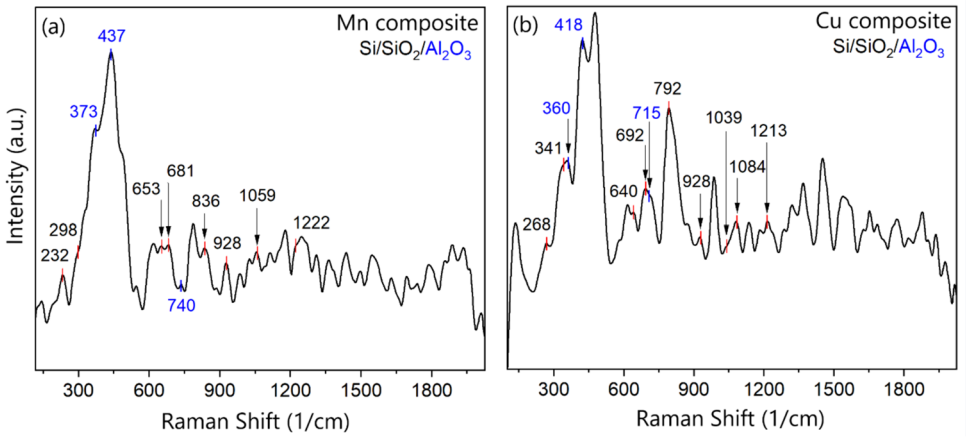

Fig. 3 Raman spectra of **a** Mn composite and **b** Cu composite

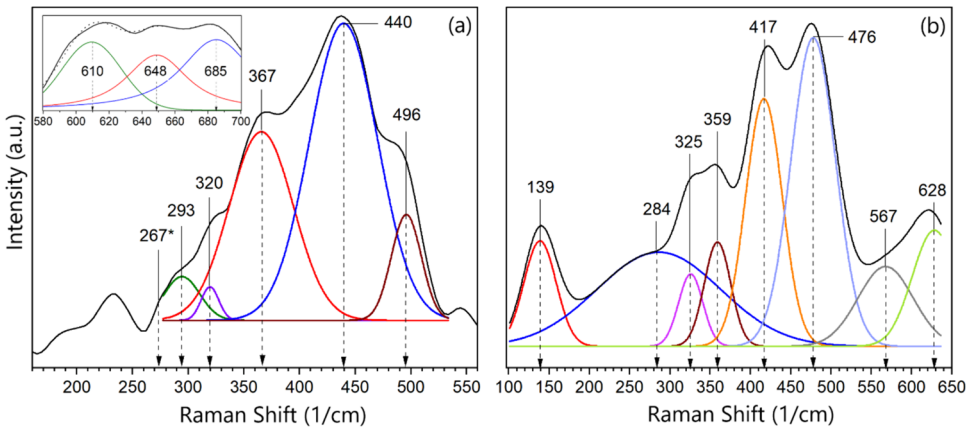

Fig. 4 Detailed spread Raman shifts of **a** Mn composite and **b** Cu composite

Table 4 Raman spectroscopy bands of Si/SiO_2 and Al_2O_3 species in initial Mn and Cu composite

Composite	Phase	Measured (Raman Shift, cm^{-1})	Reference (Raman Shift, cm^{-1})	Reference
(a) Mn composite	Si/SiO_2	232 w; 297 s; 652 s; 681 m; 835 m; 927 m; 1059 m; 1222 m	230 w; 300 s; 630; 670; 810; 930; 1030; 1090 w; 1200 w	[43, 44]
	Al_2O_3	437; 373; 740	413–420 s, 375–380 m, 758 m	[45, 46]
(b) Cu composite	Si/SiO_2	268 w; 341 s; 640; 692; 792; 928; 1039; 1084; 1213	230 w; 300 s; 630; 670; 810; 930; 1030; 1090 w; 1200 w	[43, 44]
	Al_2O_3	418; 360; 715	413–420 s, 375–380 m, 758 m	[45, 46]

during the Cu–O–Si intermediate phase in the sample. The proposed structure of Cu–O–Si was formed because the electrons of the Cu^{2+} outer layer are attracted by the Si–O bond, the electronic density decreases, and the binding energy increases [51].

As reported by Sreedharan et al. [52], it is very challenging to verify the existence of Cu–O–Si due to the lack of supporting theoretical or experimental data. Also, in this study, the proposals were based on the measured detailed Raman shifts and reported data. As mentioned earlier in this paper on the effect of microwaves on durability, bonded active metal could also increase the mechanical durability of metal composites. In the Rama spectrum, a bonded interaction was observed between Mn and Cu and SiO_2 and Al_2O_3. Also, it was proposed that the increment in SSA of the metal composites could be explained by interactions between active metal and Si and Al groups in a composite's framework.

3.5 Field emission scanning electron microscopy with energy dispersive spectroscopy

A field emission scanning electron microscope (FESEM) was conducted to investigate the microstructural pattern of metal composites. Also, energy dispersive spectroscopy (EDS) mapping was employed to confirm the active metal distribution in the metal composites. Figure 5 \presents the surface morphology of (a) the Mn (as oxide) and (b) Cu (as hydroxide) composites.

Also visually, the surface morphology of the Mn and Cu composites appears to be relatively porous, and the metal catalyst is evenly distributed compared to the SSA values in Table 2.

3.6 Calcination of kaolin with active metals

Based on the detailed characterizations described above, the preparation of precursors proceeds based on the reported reactions presented below (Eqs. 4–9) and the proposed reaction mechanisms shown in Fig. 6.

Kaolin ($Al_2O_3{\cdot}2SiO_2{\cdot}2H_2O$) [53] was calcined with $MnSO_4{\cdot}H_2O$ (aq) and $CuSO_4{\cdot}5H_2O$ (aq) as suspensions. In the case of manganese, anhydrous $MnSO_4$ was formed in the temperature range 200–300 °C and above 600 °C $MnSO_4$ decomposed to form Mn_3O_4 (i.e., $MnO{\cdot}Mn_2O_3$) (Eqs. 4 and 5) [54].

$$MnSO_4 \cdot H_2O \xrightarrow{\Delta} MnSO_4 + H_2O \tag{4}$$

$$3MnSO_4(s) \xrightarrow{\Delta} MnO \cdot Mn_2O_3(s) + 2SO_3(g) + SO_2(g) \tag{5}$$

In this study, it is proposed that during the calcination of $MnSO_4{\cdot}H_2O$ and kaolin, the Mn_3O_4/SiO_2 structure was formed in situ by a sol–gel process [55], in which Mn_3O_4 nanocrystals were dispersed in the amorphous matrix of silica in metakaolin ($Al_2Si_2O_7$) [56]. In the case of $CuSO_4{\cdot}5H_2O$, liquid water was slowly evaporated below 100 °C, and between 500 and 580 °C, dehydroxylation of internal (OH) groups occurred [47, 48]. Depending on the heating rate, four of the coordinated water molecules are released at 100–150 °C and the fifth at around 250 °C. As the temperature rises to 600–900 °C, dehydration occurs, and the copper sulfate decomposes to metallic Cu(0) and gaseous SO_2 and O_2 (Eqs. 6–9) [57].

$$CuSO_4 \cdot 5H_2O \xrightarrow{\Delta} CuSO_4 \cdot 3H_2O + 2H_2O \tag{6}$$

$$CuSO_4 \cdot 3H_2O \xrightarrow{\Delta} CuSO_4 \cdot H_2O + 2H_2O \tag{7}$$

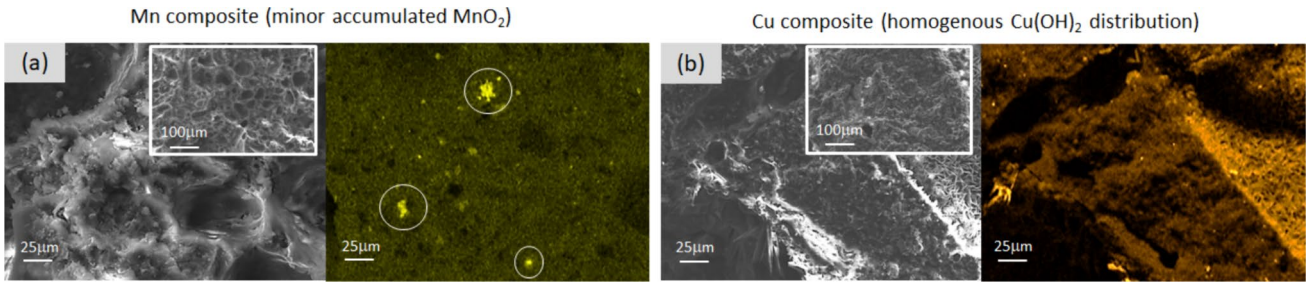

Fig. 5 FESEM and EDS mapping of **a** MnO_2 and **b** $Cu(OH)_2$ composites

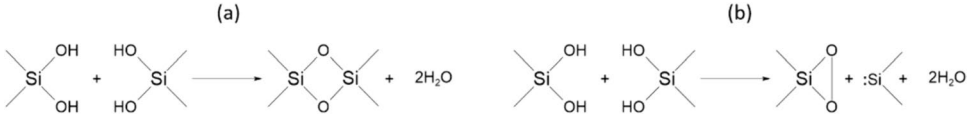

Fig. 6 Dehydroxylation of kaolin: **a** formation of an edge-sharing dimer and **b** a pair consisting of = $Si(O_2)$ and –Si

$$CuSO_4 \cdot H_2O \xrightarrow{\Delta} CuSO_4 + H_2O \quad (8)$$

$$CuSO_4 \xrightarrow{\Delta} Cu + SO_2 + O_2 \quad (9)$$

Uchino et al. reported that if normal silanol condensation appears, an edge-sharing dimer is expected to form (Fig. 6a). Also, there is another possibility that dioxasilirane (=Si(O_2)) and silylene (-Si) were generated (b) (Fig. 6b) [58].

3.7 Proposed reaction mechanism for precursors

In this paper, it is proposed that during the calcination of kaolin ($Al_2O_3{\cdot}2SiO_2{\cdot}2H_2O$) and $MnSO_4{\cdot}H_2O$ (aq), the active metal (Mn) could chemically bind with the linear ortho(sialate-siloxo) group of kaolin (Fig. 7 route a) [59]. Also, the proposed reaction mechanism between kaolin and $CuSO_4{\cdot}5H_2O$ (aq) was investigated where the active metal (Cu) and cyclic ortho(sialate-siloxo) groups of kaolin could form an in situ intermediate product of -Si–O–Cu- (Fig. 7 route b) [60]. In both reaction mechanisms, the active metal could, in a certain ratio, also appear as a form of counter cations (Cu^{2+}, Mn^{2+}, and Mn^{3+}) balancing the negative charge of Al^-. The reaction mechanisms were also based on an analysis conducted by XPS and Raman spectroscopy. XPS survey spectra and Mn2p spectra of Mn composite (Mn_3O_4) and Cu2p spectra of Cu composite ($Cu(OH)_2$) were conducted. The elemental composition of the surface of Mn and Cu composite, as well as the binding states, was detected. Also, the appearance of Mn–O–Si and Cu–O–Si bonds was observed by Raman spectroscopy, which was proposed to be located on the surface and inner parts of the porous metal composites [61, 62].

3.8 CWAO experiments

CWAO experiments were performed with the novel porous metal composites under optimal conditions (pressure, 6.0 MPa; temperature, 185 °C; initial pH, 12–13; c[catalyst], 4.0 g/L) using a 300-mL high-pressure Hastelloy C22 stainless steel reactor (Parr, Moline, IL, USA). The reactor was loaded with 160 mL of pharmaceutical wastewater (pH 12–13) and mixed at 500 rpm. During 5 h of oxidation, intermediate samples of 1.5 mL (11 pcs) were collected as a function of oxidation time. Due to the low conversion of BPA in the previous study [63], the B-MK-AAM was not examined in the CWAO of pharmaceutical wastewater. The catalytic activity of the composites was monitored by measuring the COD, TOC, and BOD of the collected intermediate samples. The experiments were repeated identically three times, and the standard deviation of COD conversion (%) was determined. Conversions of 54% and 43% were obtained for Mn and Cu composites, respectively. As can be seen in Fig. 8, the measured data were clustered very close to the average values, which gives a low standard deviation. As a reference, wet air oxidation (WAO) without added metal composite was conducted, producing a COD conversion of 15%. The initial COD of pharmaceutical wastewater was 4100 mg/L and, after oxidation with Mn and Cu composite, 1949 mg/L and 2476 mg/L, respectively.

The total concentration of organic species in the pharmaceutical wastewater was determined by TOC analysis. The TOC of the initial pharmaceutical wastewater was 1100 mg/L. Under the optimal conditions for CWAO (pressure, 6.0 MPa; temperature, 185 °C; initial pH, 12–13; c[catalyst], 4.0 g/L), TOC conversion (%) of 46% (Mn composite) and 32% (Cu composite) was achieved, respectively. When

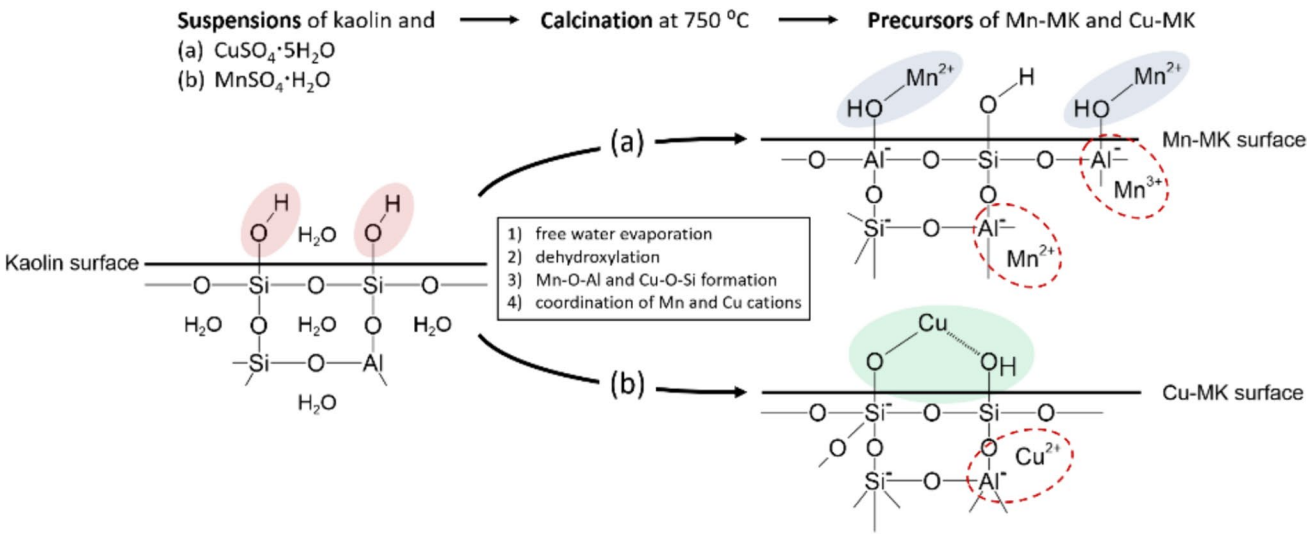

Fig. 7 Proposed reaction mechanisms during calcination of kaolin ($Al_2O_3{\cdot}2SiO_2{\cdot}2H_2O$) with (**a**) $MnSO_4{\cdot}H_2O$ and (**b**) $CuSO_4{\cdot}5H_2O$

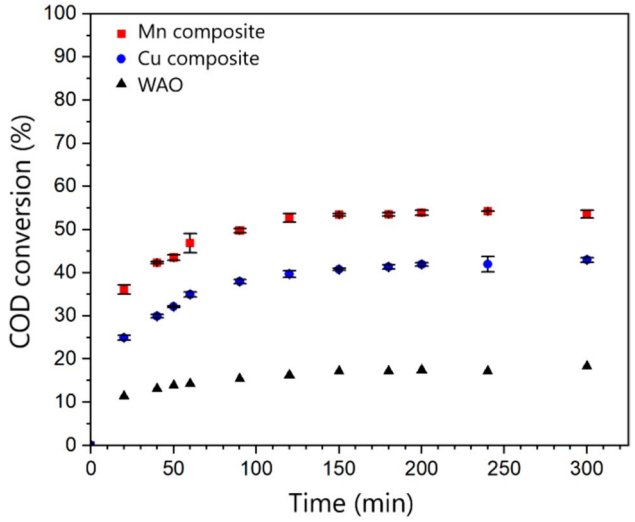

Fig. 8 Standard deviation of COD conversions (%) as a function of oxidation time with Mn and Cu composite under optimal conditions for CWAO (pressure, 6.0 MPa; temperature, 185 °C; initial pH: 12–13; and c[catalyst], 4.0 g/L), including COD conversion (%) without added metal composite (i.e., WAO) as a reference

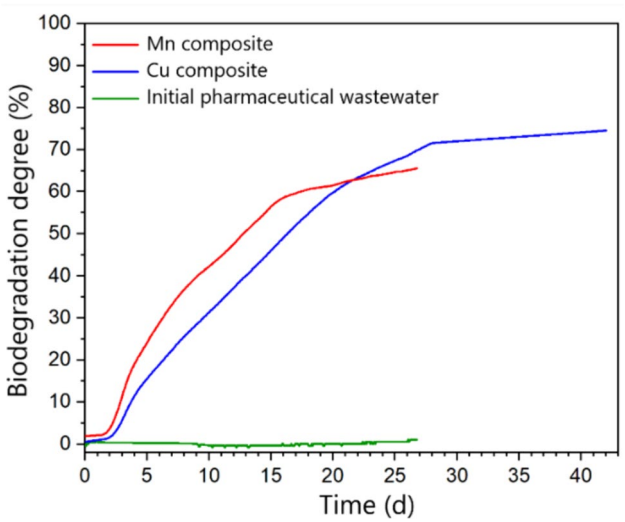

Fig. 9 Biodegradation degree (%) of oxidized pharmaceutical wastewater catalyzed by Mn and Cu composite (red and blue curves). Initial pharmaceutical wastewater as a reference (green curve)

microorganisms decompose the organic matter of the examined wastewater, they consume oxygen in the process, which determines the BOD. This indicates the amount of oxygen needed for the biological oxidation of organic matter in wastewater [64]. Initial TOC of pharmaceutical wastewater was 1100 mg/L and, after oxidation with Mn and Cu composite, 640 mg/L and 760 mg/L, respectively.

In this study, the BOD of the initial and treated pharmaceutical wastewater was determined, yielding a BOD of 23 mg/L and Mn and Cu composite of 1117 mg/L and 1414 mg/L, respectively. BOD with Mn composite stabilized after 27 days, but the measurement was continued with Cu composite for more than 2 weeks to stabilize (Fig. 8). The biodegradation degree of the initial pharmaceutical wastewater was only 2.1%, while Mn and Cu composite achieved degrees of 65% and 75%, respectively. The results indicate that the organic species of pharmaceutical wastewater can be effectively processed into a biodegradable form by CWAO with metal composites. Figure 9 presents the biodegradation degree (%) for the initial (green line) and treated process wastewater with Mn and Cu composite (red and blue lines).

3.9 Kinetic modeling

For the kinetic study, three identical CWAO experiments were performed with metal composites, and 11 individual intermediate samples were collected from each experiment. WAO without added composite was also conducted as a reference experiment. In Fig. 10, the pseudo-first order rate law is fitted to the experimental COD conversion rates of Mn composite, Cu composite, and WAO.

Experimental (exp) and calculated (calc) COD conversion percentages R_{tot} have been compared in Table 5. Also, the specific rate constant (k) for CWAO and WAO was terminated. The correlation coefficient (R^2) was used to evaluate the suitability of the fitted model.

According to the correlation coefficients, the model used showed a good correlation with the experimental data.

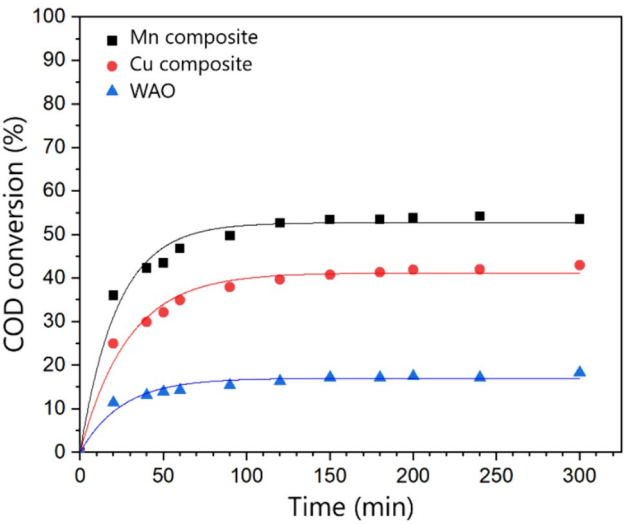

Fig. 10 Pseudo-first-order model fitted to averages of COD conversions of pharmaceutical wastewater as a function of oxidation time (5 h) with Mn and Cu composite under optimal conditions for CWAO (pressure, 6.0 MPa; temperature, 185 °C; initial pH, 12–13; c[catalyst], 4.0 g/L). COD conversion without metal composites (WAO) was used as a reference

Table 5 Experimental and calculated R_{tot} values, rate constants, and correlation coefficients for CWAO and WAO

Composite	$R_{tot\ (exp)}$ (%)	$R_{tot\ (calc)}$ (%)	k (min^{-1})	R^2
WAO	18.3	17.0	0.040	0.960
Mn composite	53.6	52.7	0.045	0.977
Cu composite	43.0	41.2	0.035	0.979

Experimental (exp) and calculated (calc) R_{tot} values are close to each other, also indicating that the pseudo-first-order model describes the experimental data well. The highest oxidation rate was achieved in the CWAO experiment, in which Mn composite was performed as a catalyzing composite. There is hardly any similar data for real wastewater in the literature, but the *k*-values obtained in this work are of the same order of magnitude as those obtained with a Pt catalyst for a model solution of bisphenol A [28].

3.10 Recycled composites

Four cycles were conducted for metal composites in CWAO to investigate chemical stability and catalytic activity in pharmaceutical wastewater. In Fig. 11, the COD conversions (%) of recycled Mn and Cu composite were compared. Each cycle was conducted under the optimal conditions for CWAO (pressure, 6.0 MPa; temperature, 185 °C; initial pH, 12–13; c[catalyst], 4.0 g/L). As can be seen from the bar graph, no major changes were observed in the catalytic activity, indicating the stable mechanical and chemical durability of the metal composites. In terms of the cost-effectiveness

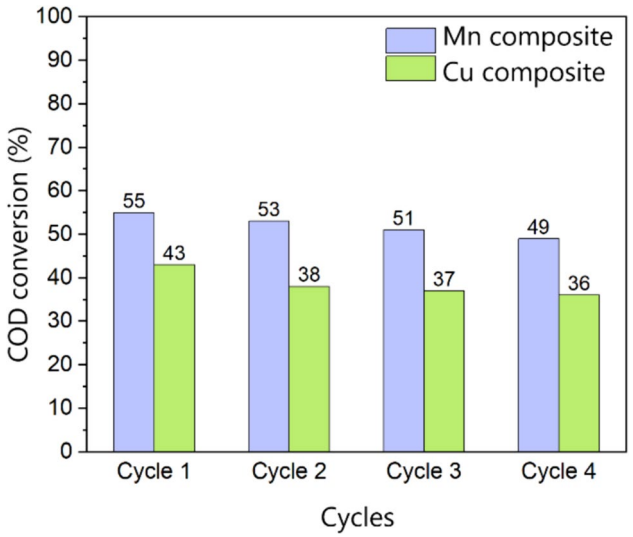

Fig. 11 COD conversions (%) of pharmaceutical wastewater recycled (1–4) with Mn and Cu composite under the optimal conditions for CWAO (pressure, 6.0 MPa; temperature, 185 °C; initial pH, 12–13; c[catalyst], 4.0 g/L)

and ecology of metal composites, it is important that reusability, mechanical durability, and catalytic activity remain as high as possible.

3.11 Characterization of recycled composites

Determined N_2 adsorption-desorption isotherms of initial and recycled metal composites (see 3. Supplementary Material: Isotherm of Recycled Mn and Cu composite) show type IV isotherms with distinguishing hysteresis loops corresponding to mesoporous materials, which correspond to the percentage values of the pore size distribution (%) shown earlier in Table 2. A minor decrease in K content was observed in the recycled Mn and Cu composite due to the minor leaching of potassium during oxidation. The reusability and sufficient activity of metal composites depend on the stability of the materials. During oxidation, the composition of metal composites degenerates, causing mass loss. In this study, after 5 h of CWAO, an average of 1.2 wt.% of the material was eroded due to the high rate of mixing and solution flow. After CWAO, the metal content (wt.%) of recycled metal composites was analyzed by ICP-OES. Initial metal composites were as a reference. Leached metal content (wt.%) is marked as a negative value (Table 6).

3.12 Crystal phases of initial and recycled metal composites

The crystallographic structure and chemical composition of metal composites were determined by XRD. The XRD patterns of the initial and recycled (a) Mn composite and (b) Cu composites are presented in Fig. 12. The main peaks of MnO_2 were located at 15, 37°, 39°, 40°, and 51° [65]. Also, the main peaks of MnO were located at 39° and 59° and Mn_3O_4 at 40° and 44° [66]. The same mean peaks of both Mn oxides were in the three-times-cycled Mn composite, but a strong signal at 15° occurred. This indicates an increase in the MnO_2 content on the surface of the cyclized Mn composite. The main peaks of $Cu(OH)_2$ in the initial Cu composite were located at 17°, 21°, 35°, 41°, 50°, and 66° in

Table 6 Metal content (wt.%) of initial and recycled Mn and Cu composites

Composite	Al wt.%	Si	K	Mn	Cu
Mn composite (initial)	12.7	19.7	3.90	10.7	0.05
Mn composite (recycled)	11.7	18.7	1.52	8.9	0.02
Difference (leached)	−1.0	−1.0	−2.38	−1.80	−0.03
Cu composite (initial)	13.1	20.0	4.70	< < 0	10.9
Cu composite recycled)	12.4	19.7	1.63	< < 0	6.54
Difference (leached)	−0.7	−0.3	−3.07	< < 0	−4.36

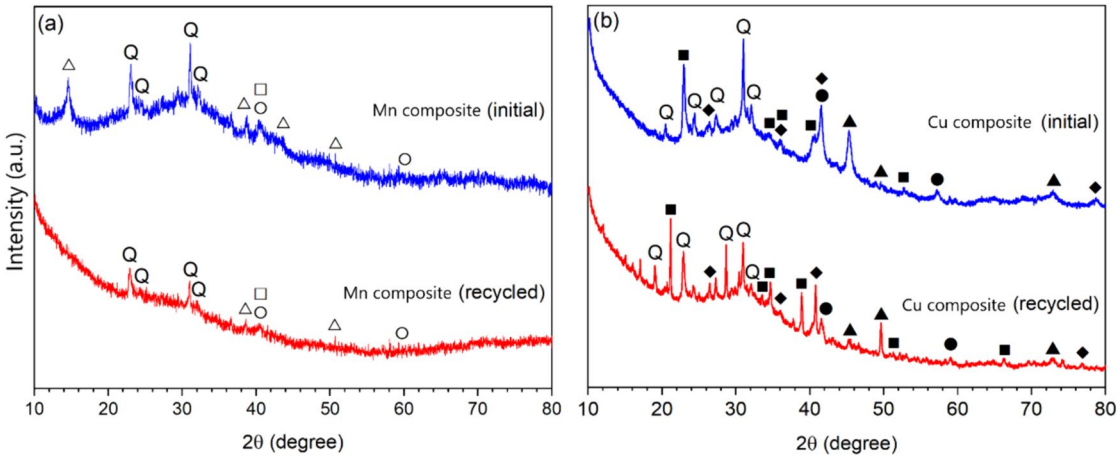

Fig. 12 X-ray diffractograms of the initial and recycled **a** Mn composite and **b** Cu composite. Legend: triangle = MnO_2, square = Mn_3O_4, circle = MnO, black square = $Cu(OH)_2$, black diamond = Cu_2O, black circle = CuO, and black triangle = Cu(0) (metallic); Q = quartz

2θ, corresponding to orthorhombic $Cu(OH)_2$ (ICDD 00-35-0505) [20, 67]. The main peaks of metallic Cu(0) were located at 45°, 50°, and 73° [68]. These results correspond to the preparation process of Cu composite via calcination and posttreatment. The main peaks of Cu_2O and CuO in recycled Cu composite were located at 26°, 36°, and 79° (ICDD 05-0667) [69] and 32°, 42°, and 57° (ICDD 48-1548) [67], respectively. Broadband between 24 and 34° in both the XRD of Mn and Cu composite indicates the amorphous structure of the composites [70]. Due to metakaolin and active metal-based precursors (Mn- and Cu-MK), some characteristic signals of Mn and Cu overlapped by a wide amorphous region of metakaolin between 20 and 35° and were not clearly detected in the diffractograms. The center of the amorphous diffraction "hump" of metakaolin was located at roughly 2θ 27° (see 4. Supplementary Material: XRD of metakaolin (MK)) [71].

4 Conclusion

In this study, ecological and low-cost porous metakaolin-based alkali-activated composites with transition metals (Mn and Cu composite) were produced to decompose organic species of pharmaceutical wastewater in CWAO. Microwaves and a specific pressurized, sealed Teflon cylinder were used to cure alkali-activated paste and produce mechanically durable metal composites. The chemical and mechanical properties of Mn and Cu composite were determined, and the performance in the CWAO of pharmaceutical wastewater was investigated, resulting in an excellent increase in the biodegradability of organics (65% and 75%). The metal composites indicated slight leaching of metals during the oxidation and maintained excellent stability and catalytic activity during the cycling experiments. The reaction mechanisms during the calcination of suspension of kaolin and active metals were investigated in detail, including various analyses. Based on the results, it is proposed that both metals, Mn and Cu, were chemically bound to the amorphous structure of metakaolin during the dehydroxylation at 500–750 °C. The results obtained in this study show that even under mild reaction conditions in CWAO (compared to thermal oxidation) with the novel metal composites, organic molecules in pharmaceutical wastewater can be decomposed into being biodegradable and less harmful to the environment.

5 Further studies

In further studies, transition metal composites could also be bi- or tri-metal composites, where the amounts of metals are precisely optimized. In addition, the mechanical durability of metal composites could be improved by adding cellulose fibers or steel wool fibers to the paste during the preparation process and supporting the whole network structure. Precursors could also be prepared from other raw materials, such as alumino-silicon-containing porcelain and glass and steel wool.

Instead of molds, metal composites could also be produced with automated spray technology by forming thin alkali-activated films, like a laminate, and stacked on top of each other. If desired, metal catalyst layers can also be produced between the laminates. Spraying can be conducted by changing the spray angle, which creates a different texture on the surface of each film and might increase the porosity of metal composites.

Supplementary Information The online version contains supplementary material available at https://doi.org/10.1007/s42114-024-00982-8.

Acknowledgements The authors thank the staff of the University of Oulu's Center of Microscopy and Nanotechnology for their assistance during the elementary and XPS analyses. Thanks to Markus Väyrynen, Juhani Väisänen, Sari Tuikkanen, Riikka Koski, and Davide Bergna for their assistance in this experimentation.

Author contributions Conceptualization, M.P.C.; methodology, M.P.C.; software, M.P.C., A.H., T.K.; T.H.; H.P.; experimental, M.P.C., A.H., T.K.; T.H.; H.P.; investigation, M.P.C., A.H., T.K; T.H.; H.P.; data curation, M.P.C.; writing original draft preparation, M.P.C., A.H., T.K.; T.H.; H.P.; writing review and editing, all authors; visualization, M.P.C.; supervision, A.H. and U.L.; funding acquisition, M.P.C., U.L. All authors have read and agreed the published version of the manuscript.

Funding Open Access funding provided by University of Oulu (including Oulu University Hospital). This work was financially supported by the Maa- ja vesitekniikan tuki ry, the KAUTE Foundation, and the University of Oulu Graduate School (UniOGS).

Declarations

Conflict of interest The authors declare no competing interests.

Open Access This article is licensed under a Creative Commons Attribution 4.0 International License, which permits use, sharing, adaptation, distribution and reproduction in any medium or format, as long as you give appropriate credit to the original author(s) and the source, provide a link to the Creative Commons licence, and indicate if changes were made. The images or other third party material in this article are included in the article's Creative Commons licence, unless indicated otherwise in a credit line to the material. If material is not included in the article's Creative Commons licence and your intended use is not permitted by statutory regulation or exceeds the permitted use, you will need to obtain permission directly from the copyright holder. To view a copy of this licence, visit http://creativecommons.org/licenses/by/4.0/.

References

1. Valdez-Carrillo M, Abrell L, Ramírez-Hernández J, Reyes-López JA, Carreón-Diazconti C (2020) Pharmaceuticals as emerging contaminants in the aquatic environment of Latin America: a review. Environ Sci Pollut Res 27:44863–44891. https://doi.org/10.1007/s11356-020-10842-9
2. Patel M, Kumar R, Kishor K, Mlsna T, Pittman CU, Mohan D (2019) Pharmaceuticals of emerging concern in aquatic systems: chemistry, occurrence, effects, and removal methods. Chem Rev 119:3510–3673. https://doi.org/10.1021/acs.chemrev.8b00299
3. Sharma J, Joshi M, Bhatnagar A, Chaurasia AK, Nigam S (2022) Pharmaceutical residues: one of the significant problems in achieving 'clean water for all' and its solution. Environ Res. https://doi.org/10.1016/j.envres.2022.114219
4. Janda R, Ukić Š, Mikulec N, Vitale K (2021) Bisphenol A – an environmental and human threat. Agric Conspec Sci 86:295–304
5. Levec J, Pintar A (2007) Catalytic wet-air oxidation processes: a review. Catal Today 124:172–184. https://doi.org/10.1016/j.cattod.2007.03.035
6. Kim KH, Ihm SK (2011) Heterogeneous catalytic wet air oxidation of refractory organic pollutants in industrial wastewaters: a review. J Hazard Mater 186:16–34. https://doi.org/10.1016/j.jhazmat.2010.11.011
7. Zhang Y, Chen S, Chen X, Huang J, Chen L, Wu T, Huang J, Liu Y (2020) CWAO Technology for the treatment of refractory-biodegradable organic wastewater. J Phys Conf Ser. https://doi.org/10.1088/1742-6596/1549/2/022041
8. Castaldo R, Iuliano M, Cocca M, Ambrogi V, Gentile G, Sarno M (2019) A new route for low pressure and temperature CWAO: a PtRu/MoS2_hyper-crosslinked nanocomposite. Nanomaterials. https://doi.org/10.3390/nano9101477
9. Zhang Z, Yang R, Gao Y, Zhao Y, Wang J, Huang L, Guo J, Zhou T, Lu P, Guo Z, Wang Q (2014) Novel Na2Mo4O13/α-MoO3hybrid material as highly efficient CWAO catalyst for dye degradation at ambient conditions. Sci Rep 4:1–9. https://doi.org/10.1038/srep06797
10. Fu J, Yang K, Ma C, Zhang N, Gai H, Zheng J, Chen BH (2016) Bimetallic Ru-Cu as a highly active, selective and stable catalyst for catalytic wet oxidation of aqueous ammonia to nitrogen. Appl Catal B Environ 184:216–222. https://doi.org/10.1016/j.apcatb.2015.11.031
11. Sushma AK (2018) Saroha, Biodegradability enhancement of industrial organic raffinate containing pyridine and its derivatives by CWAO using ceria promoted MnOx/Al2O3 catalyst at atmospheric pressure. Chem Eng J 334:985–994. https://doi.org/10.1016/j.cej.2017.10.100
12. Feng B, Hao L, Deng C, Wang J, Song H, Xiao M, Huang T, Zhu Q, Gai H (2023) A highly hydrothermal stable copper-based catalyst for catalytic wet air oxidation of m-cresol in coal chemical wastewater, Chinese. J Chem Eng 57:338–348. https://doi.org/10.1016/j.cjche.2022.11.006
13. Papa E, Medri V, Kpogbemabou D, Morinière V, Laumonier J, Vaccari A, Rossignol S (2016) Porosity and insulating properties of silica-fume based foams. Energy Build 131:223–232. https://doi.org/10.1016/j.enbuild.2016.09.031
14. Zhang Z, Provis JL, Reid A, Wang H (2015) Mechanical, thermal insulation, thermal resistance and acoustic absorption properties of geopolymer foam concrete. Cem Concr Compos 62:97–105. https://doi.org/10.1016/j.cemconcomp.2015.03.013
15. Zhou Y, Zhang H, Yan Y (2018) Catalytic oxidation of ethyl acetate over CuO/ZSM-5 catalysts: effect of preparation method. J Taiwan Inst Chem Eng 84:162–172. https://doi.org/10.1016/j.jtice.2018.01.016
16. Wang Y, Yang W, Yin X, Liu Y (2016) The role of Mn-doping for catalytic ozonation of phenol using Mn/γ-Al2O3 nanocatalyst: performance and mechanism. J Environ Chem Eng 4:3415–3425. https://doi.org/10.1016/j.jece.2016.07.016
17. Roshani B, McMaster I, Rezaei E, Soltan J (2014) Catalytic ozonation of benzotriazole over alumina supported transition metal oxide catalysts in water. Sep Purif Technol 135:158–164. https://doi.org/10.1016/j.seppur.2014.08.011
18. Deng J, Xu M, Chen Y, Li J, Qiu C, Li X, Zhou S (2019) Highly-efficient removal of norfloxacin with nanoscale zero-valent copper activated persulfate at mild temperature. Chem Eng J 366:491–503. https://doi.org/10.1016/j.cej.2019.02.073
19. Zhang MT, Chen Z, Kang P, Meyer TJ (2013) Electrocatalytic water oxidation with a copper(II) polypeptide complex. J Am Chem Soc 135:2048–2051. https://doi.org/10.1021/ja3097515
20. Cui S, Liu X, Sun Z, Du P (2016) Noble metal-free copper hydroxide as an active and robust electrocatalyst for water oxidation at weakly basic pH. ACS Sustain Chem Eng 4:2593–2600. https://doi.org/10.1021/acssuschemeng.6b00067
21. Adegbesan CD, Daniel S, Monguen CKF, Otieno HN, Tian ZY (2024) Catalytically active Cu-Fe/Kaolin hybrid catalyst for semi-hydrogenation of acetylene. Eng Sci. https://doi.org/10.30919/es1148
22. El-Moghny MWA, El-Desoky HM, El-Nagar AM, El-Hafez NAA, Sharaka HK, Abouellaban SA (2022) Thermal treatment of Kalabsha kaolin deposits, south of the Western Desert, Egypt: contribution to geopolymer production as green building materials. Arab J Geosci. https://doi.org/10.1007/s12517-022-09637-8

23. Christophliemk MP, Heponiemi A, Hu T, Lassi U (2023) Preparation of porous and durable metakaolin-based alkali-activated materials with active metal as composites for catalytic wet air oxidation. Top Catal 66:1427–1439. https://doi.org/10.1007/s11244-022-01775-3
24. Christophliemk MP, Heponiemi A, Hu T, Lassi U (2024) Preparation of porous metakaolin-based alkali-activated materials by microwave curing as supports for non-noble metal catalysts. Next Mater 3:100039. https://doi.org/10.1016/j.nxmate.2023.100039
25. Christophliemk MP, Pikkarainen AT, Heponiemi A, Tuomikoski S, Runtti H, Hu T, Kantola AM, Lassi U (2022) Preparation and characterization of porous and stable sodium- and potassium-based alkali activated material (AAM). Appl Clay Sci. https://doi.org/10.1016/j.clay.2022.106697
26. Landers J, Gor GY, Neimark AV (2013) Density functional theory methods for characterization of porous materials. Colloids Surfaces A Physicochem Eng Asp 437:3–32. https://doi.org/10.1016/j.colsurfa.2013.01.007
27. Thommes M, Smarsly B, Groenewolt M, Ravikovitch PI, Neimark AV (2006) Adsorption hysteresis of nitrogen and argon in pore networks and characterization of novel micro- and mesoporous silicas. Langmuir 22:756–764. https://doi.org/10.1021/la051686h
28. Heponiemi A, Azalim S, Hu T, Vielma T, Lassi U (2019) Efficient removal of bisphenol A from wastewaters: Catalytic wet air oxidation with Pt catalysts supported on Ce and Ce-Ti mixed oxides. AIMS Mater Sci 6:25–44. https://doi.org/10.3934/matersci.2019.1.25
29. Heponiemi A, Rahikka L, Lassi U, Kuokkanen T (2011) Catalytic oxidation of industrial wastewater under mild conditions. Top Catal 54:1034–1041. https://doi.org/10.1007/s11244-011-9723-9
30. Nyborg L, Cao Y (2022) Surface chemical and geometrical properties of pure copper powder intended for binder jetting and sintering. Surf Interface Anal 54:944–953. https://doi.org/10.1002/sia.7107
31. Jumrat S, Chatveera B, Rattanadecho P (2011) Dielectric properties and temperature profile of fly ash-based geopolymer mortar. Int Commun Heat Mass Transf 38:242–248. https://doi.org/10.1016/j.icheatmasstransfer.2010.11.020
32. Somaratna J, Ravikumar D, Neithalath N (2010) Response of alkali activated fly ash mortars to microwave curing. Cem Concr Res 40:1688–1696. https://doi.org/10.1016/j.cemconres.2010.08.010
33. Tanaka H, Fujii A, Fujimoto S, Tanaka Y (2008) Microwave-assisted two-step process for the synthesis of a single-phase Na-A zeolite from coal fly ash. Adv Powder Technol 19:83–94. https://doi.org/10.1163/156855208X291783
34. Chindaprasirt P, Rattanasak U, Taebuanhuad S (2013) Role of microwave radiation in curing the fly ash geopolymer. Adv Powder Technol 24:703–707. https://doi.org/10.1016/j.apt.2012.12.005
35. Cano E, Torres CL, Bastidas JM (2001) An XPS study of copper corrosion originated by formic acid vapour at 40% and 80% relative humidity. Werkst Korros 52:667–676. https://doi.org/10.1002/1521-4176(200109)52:9%3c667::aid-maco667%3e3.0.co;2-h
36. Moses Ezhil Raj A, Victoria SG, Jothy VB, Ravidhas C, Wollschläger J, Suendorf M, Neumann M, Jayachandran M, Sanjeeviraja C (2010) XRD and XPS characterization of mixed valence Mn 3 O 4 hausmannite thin films prepared by chemical spray pyrolysis technique. Appl Surf Sci 256:2920–2926. https://doi.org/10.1016/j.apsusc.2009.11.051
37. Wang M, Chen K, Liu J, He Q, Li G, Li F (2018) Efficiently enhancing electrocatalytic activity of α-MnO2 nanorods/N-doped ketjenblack carbon for oxygen reduction reaction and oxygen evolution reaction using facile regulated hydrothermal treatment. Catalysts. https://doi.org/10.3390/catal8040138
38. Guo J, Zhang X, Du X, Zhang F (2017) A Mn3O4 nano-wall array based binder-free cathode for high performance lithium-sulfur batteries. J Mater Chem A 5:6447–6454. https://doi.org/10.1039/c7ta00475c
39. Yan J, Fan Z, Wei T, Cheng J, Shao B, Wang K, Song L, Zhang M (2009) Carbon nanotube/MnO2 composites synthesized by microwave-assisted method for supercapacitors with high power and energy densities. J Power Sources 194:1202–1207. https://doi.org/10.1016/j.jpowsour.2009.06.006
40. Biesinger MC (2017) Advanced analysis of copper X-ray photoelectron spectra. Surf Interface Anal 49:1325–1334. https://doi.org/10.1002/sia.6239
41. Biesinger MC, Lau LWM, Gerson AR, Smart RSC (2010) Resolving surface chemical states in XPS analysis of first row transition metals, oxides and hydroxides: Sc, Ti, V, Cu and Zn. Appl Surf Sci 257:887–898. https://doi.org/10.1016/j.apsusc.2010.07.086
42. Abdolmohammad-Zadeh H, Javan Z (2015) Silica-coated Mn3O4 nanoparticles coated with an ionic liquid for use in solid phase extraction of silver(I) ions prior to their determination by AAS. Microchim Acta 182:1447–1456. https://doi.org/10.1007/s00604-015-1468-x
43. Borowicz P, Taube A, Rzodkiewicz W, Latek M, Gierałtowska S (2013) Raman spectra of high-κ dielectric layers investigated with micro-raman spectroscopy comparison with silicon dioxide. Sci World J. https://doi.org/10.1155/2013/208081
44. Mankad V, Gupta SK, Jha PK, Ovsyuk NN, Kachurin GA (2012) Low-frequency Raman scattering from Si/Ge nanocrystals in different matrixes caused by acoustic phonon quantization. J Appl Phys. https://doi.org/10.1063/1.4747933
45. Gyakwaa F, Alatarvas T, Shu Q, Aula M, Fabritius T (2021) Characterization of synthetic non-metallic inclusions. Metals 11:1549. https://doi.org/10.3390/met11101549
46. Wan KS, Tochino S, Zhu WL, Ohtsuka S, Pezzotti G (2010) Quantitative evaluation of probe response functions for Raman and fluorescence bands of single-crystalline and polycrystalline Al 2O3. J Phys D Appl Phys. https://doi.org/10.1088/0022-3727/43/20/205501
47. Tite T, Shu GJ, Chou FC, Chang YM (2010) Structural and thermal properties of MnSi single crystal. Appl Phys Lett 97:1–4. https://doi.org/10.1063/1.3464980
48. Hayashi K, Ishii K, Kawasaki C, Honda R, Miyazaki Y (2018) Preparation and optical properties of higher manganese silicide, (Mn, Fe)Si γ, thin films. Appl Surf Sci 458:700–704. https://doi.org/10.1016/j.apsusc.2018.07.141
49. Zhang L, Zhang F, Liu M, Hu X (2017) Novel sustainable geopolymer based syntactic foams: an eco-friendly alternative to polymer based syntactic foams. Chem Eng J 313:74–82. https://doi.org/10.1016/J.CEJ.2016.12.046
50. Choudhary S, Sarma JVN, Pande S, Ababou-Girard S, Turban P, Lepine B, Gangopadhyay S (2018) Oxidation mechanism of thin Cu films: a gateway towards the formation of single oxide phase. AIP Adv. https://doi.org/10.1063/1.5028407
51. Li H, Ban L, Wang Z, Meng P, Zhang Y, Wu R, Zhao Y (2019) Regulation of Cu species in CuO/SiO2 and its structural evolution in ethynylation reaction. Nanomaterials. https://doi.org/10.3390/nano9060842
52. Sreedharan R, Mohan M, Saini S, Roy A, Bhattacharjee K (2021) Intermediate Cu-O-Si phase in the Cu-SiO2/Si(111) system: growth, elemental, and electrical studies. ACS Omega 6:23826–23836. https://doi.org/10.1021/acsomega.1c02646
53. Zhang ZH, Zhu HJ, Zhou CH, Wang H (2016) Geopolymer from kaolin in China: an overview. Appl Clay Sci 119:31–41. https://doi.org/10.1016/j.clay.2015.04.023
54. Warner TE, Bancells MM, Lund PB, Lund FW, Ravnsbæk DB (2019) On the thermal stability of manganese(II) sulfate and its

reaction with zeolite A to form the sodalite Na6Mn2[Al6Si6O24](SO4)2. J Solid State Chem 277:434–440. https://doi.org/10.1016/j.jssc.2019.06.038
55. Davar F, Salavati-Niasari M, Mir N, Saberyan K, Monemzadeh M, Ahmadi E (2010) Thermal decomposition route for synthesis of Mn3O4 nanoparticles in presence of a novel precursor. Polyhedron 29:1747–1753. https://doi.org/10.1016/j.poly.2010.02.026
56. El-Diadamony H, Amer AA, Sokkary TM, El-Hoseny S (2018) Hydration and characteristics of metakaolin pozzolanic cement pastes. HBRC J 14:150–158. https://doi.org/10.1016/j.hbrcj.2015.05.005
57. Danon A, Saig A, Finkelstein Y, Koresh JE (2005) A new route of oxygen isotope exchange in the solid phase: demonstration in CuSO4·5H2O. J Phys Chem B 109:21197–21201. https://doi.org/10.1021/jp051000u
58. Uchino T, Kurumoto N, Sagawa N (2006) Structure and formation mechanism of blue-light-emitting centers in silicon and silica-based nanostructured materials. Phys Rev B - Condens Matter Mater Phys. https://doi.org/10.1103/PhysRevB.73.233203
59. Allen N, Dai C, Hu Y, Kubicki JD, Kabengi N (2019) Adsorption study of Al3+, Cr3+, and Mn2+ onto quartz and corundum using flow microcalorimetry, quartz crystal microbalance, and density functional theory. ACS Earth Sp Chem 3:432–441. https://doi.org/10.1021/acsearthspacechem.8b00148
60. Cho DY, Tappertzhofen S, Waser R, Valov I (2013) Bond nature of active metal ions in SiO2-based electrochemical metallization memory cells. Nanoscale 5:1781–1784. https://doi.org/10.1039/c3nr34148h
61. Jawaid M, Swain SK (2017) Bionanocomposites for packaging applications. Bionanocomposites Packag Appl. https://doi.org/10.1007/978-3-319-67319-6
62. Wen J, Ma T, Zhang W, Van Duin ACT, Van Duin DM, Hu Y, Lu X (2019) Atomistic insights into Cu chemical mechanical polishing mechanism in aqueous hydrogen peroxide and glycine: ReaxFF reactive molecular dynamics simulations. J Phys Chem C 123:26467–26474. https://doi.org/10.1021/acs.jpcc.9b08466
63. Christophliemk MP, Heponiemi A, Hu T, Lassi U (2022) Preparation of porous and durable metakaolin-based alkali-activated materials with active metal as composites for catalytic wet air oxidation. Top Catal. https://doi.org/10.1007/s11244-022-01775-3
64. Dhall P, Siddiqi TO, Ahmad A, Kumar R, Kumar A (2012) Restructuring BOD: COD ratio of dairy milk industrial wastewaters in BOD analysis by formulating a specific microbial seed. Sci World J. https://doi.org/10.1100/2012/105712
65. Kumar P, Khan MQ, Khan RA, Ahmad K, Kim H (2022) Hydrothermal synthesis of MnO2/reduced graphene oxide composite for 4-nitrophenol sensing applications. Inorganics. https://doi.org/10.3390/inorganics10120219
66. Jankovský O, Sedmidubský D, Šimek P, Sofer Z, Ulbrich P, Bartuněk V (2015) Synthesis of MnO, Mn2O3 and Mn3O4 nanocrystal clusters by thermal decomposition of manganese glycerolate. Ceram Int 41:595–601. https://doi.org/10.1016/j.ceramint.2014.08.108
67. Li Z, Xin Y, Zhang Z, Wu H, Wang P (2015) Rational design of binder-free noble metal/metal oxide arrays with nanocauliflower structure for wide linear range nonenzymatic glucose detection. Sci Rep 5:1–10. https://doi.org/10.1038/srep10617
68. Kanuchova M, Kozakova L, Drabova M, Sisol M, Estokova A, Kanuch J, Skvarla J (2015) Monitoring and characterization of creation of geopolymers prepared from fly ash and metakaolin by X-ray photoelectron spectroscopy method. Environ Prog Sustain Energy 34:841–849. https://doi.org/10.1002/ep.12068
69. Kooti M, Matouri L (2010) Fabrication of nanosized cuprous oxide using fehling's solution. Sci Iran 17:73–78
70. Ivanovic M, Kljajevic L, Nenadovic M, Bundaleski N, Vukanac I, Todorovic B, Nenadovic S (2018) Physicochemical and radiological characterization of kaolin and its polymerization products. Mater Constr. https://doi.org/10.3989/mc.2018.00517
71. Djobo JNY, Tchadjié LN, Tchakoute HK, Kenne BBD, Elimbi A, Njopwouo D (2014) Synthesis of geopolymer composites from a mixture of volcanic scoria and metakaolin. J Asian Ceram Soc 2:387–398. https://doi.org/10.1016/j.jascer.2014.08.003

Publisher's Note Springer Nature remains neutral with regard to jurisdictional claims in published maps and institutional affiliations.